

## **Wave interactions with circular ice ridge embedded in level ice**

**Sourav Mandal<sup>a, b</sup>, Adrian Wing-Keung Law<sup>b, c, \*</sup>, Hayley H. Shen<sup>b, d</sup>**

<sup>a</sup> Ocean Engineering Division, CSIR-National Institute of Oceanography, Goa 403004, India

<sup>b</sup> Environmental Process Modelling Centre, Nanyang Environment and Water Research Institute, Nanyang Technological University, Clean Tech One, 637141, Singapore

<sup>c</sup> School of Civil and Environmental Engineering, Nanyang Technological University, 639798, Singapore

<sup>d</sup> 132 Rowley Laboratories, Civil and Environmental Engineering, Clarkson University, Potsdam, NY 13699-5710, USA

### **Abstract**

The present study examines the wave interactions with a circular elastic body trapped within a thin cover of sea ice of substantial extent. This configuration is an idealization of an ice ridge embedded in a field of level ice. The ice cover and ice ridge are both modeled as thin elastic plates. Two independent approaches are used. The first approach ignores the finite draft, and a closed-form solution is obtained by taking the inner product with respect to the eigenfunctions for the ice-covered region. The second approach includes the finite draft, and a least square approximation method is adopted along with the matching of velocity and pressure between the ice cover and ice ridge. Using the second approach, the surge force on the ice ridge, its deflection and the bending moments over the surface are then computed for various ridge configurations and wave characteristics. The submergence of the ridge is found to have a considerable effect on the deflection as well as the surge force in the presence of the ice cover. The results show that the level ice significantly affects the ice ridge response to shorter waves. It is found that the ridge embedded in ice cover experiences larger bending moments compared to the open water case. The results from the present study can help estimate the response of ice ridges to incoming waves, as well as aid in the design of offshore cylindrical structures embedded in level ice.

**Keywords:** Flexural-gravity waves, ice ridge, level ice, deflection, surge force, bending moment.

\* Corresponding author at: School of Civil and Environmental Engineering, Nanyang Technological University, 639798, Singapore.

Email addresses: [sourav@nio.org](mailto:sourav@nio.org) (S. Mandal); [CWKLAW@ntu.edu.sg](mailto:CWKLAW@ntu.edu.sg) (A-W-K Law); [hshen@clarkson.edu](mailto:hshen@clarkson.edu) (H.H. Shen)

## 1. Introduction

Ice ridge is a natural formation of sea ice under convergence. The ridging process produces massive piles of ice that can reach tens of meters in thickness (Kvadsheim 2014). These ridges are integral parts of the Arctic pack ice, and they move with the rest of ice cover in the Arctic basin. When they reach the marginal ice zone (i.e. MIZ, the region between a continuous pack ice and the open ocean), their threat to shipping and offshore structures may be comparable to those of bergy bits. The ice ridge is much more likely subjected to wave forces in MIZ than when it is in the interior pack ice, and its motion and deformation can be significantly influenced by the additional forcing.

During the last three decades, there is a growing interest in wave-ice interactions (see Squire 1995, 2007). Meylan and Squire (1996) studied the response of a thin circular ice floe to long-crested ocean waves. Later, Meylan (2002) developed a more general model to investigate the motion and bending of a solitary ice floe in the case of infinite water depth. On the other hand, Zilman and Miloh (2000) analytically investigated the response of a circular ice floe using a linearized shallow water theory. Tsubogo (2001) used an advanced Boundary Element Method (BEM) to analyze floating elastic plates. Peter et al. (2004) presented an extension of Zilman and Miloh (2000) to the case where the water depth is finite using the orthogonal properties of eigenfunctions. Andrianov and Hermans (2005) studied in details the hydroelastic responses of a floating circular annular plate in a range of wave fields. Bennetts and Williams (2010) analyzed wave scattering by an ice floe of arbitrary shape. Montiel et al. (2013) investigated the hydroelastic response of a floating circular disc and compared their results with the data obtained from the wave basin experiments. Mondal et al. (2014) derived the closed form solution for the problem presented in Peter et al. (2004) in the ice-covered region. They also derived closed form solutions for the case of stratified fluid under both shallow and finite water depth. In all the theories above, the submergence of circular ice floe is neglected by assuming that the wavelength is much larger than the ice thickness. Therefore, the boundary conditions are applied at the mean water level rather than at the actual wetted surface of the ice floe.

In two-dimensional conditions, Squire and Dixon (2001) previously modeled the flexural gravity wave interaction with an iceberg embedded in shore fast sea ice using the Green's function method. The current study deals with the same structural configuration but in three-dimensional conditions instead. Least square approximation method is adopted to evaluate the effect of submergence of the ice ridge. It should be noted that other researchers had previously investigated the reflection and transmission of flexural-gravity waves with a sudden change of ice properties. Bennetts et al. (2007) used a variational approach invoking the Rayleigh-Ritz method to investigate the wave scattering by a non-uniform ice sheet of variable thickness. Williams and Squire (2008) incorporated the changes of

submergence among three adjoining plates. Andrianov and Hermans (2006) studied the diffraction of incident surface water waves by a very large floating structure considering the draft. Williams and Porter (2009) investigated the effect of submergence on the scattering by the interface between two semi-infinite sheets.

Besides the above studies which were ice related, there were also extensive relevant work reported in the offshore engineering literature. Most of these studies focused on the prediction of wave loads on a circular rigid structure under the action of waves in open water. The consideration of draft is normally included in these studies (see Garrett 1971; Linton and McIver 2001; Finnegan et al. 2013; Mandal et al. 2013). However, to the best of the authors' knowledge, the analysis of the present configuration has not been reported so far in both of the ice and offshore engineering literature.

In this study, we analyze analytically the wave forcing on a circular ice ridge embedded in an ice sheet allowing for the effect of submergence. Two types of conditions are considered: (i) frozen edge and (ii) free edge. We analyze two independent approaches. In the first approach, a closed form solution is obtained using the inner product with respect to the eigenfunctions for the ice-covered region without the effect of submergence of ice ridge. In the second approach, the finite draft is treated by matching the velocity and pressure between the ice ridge and the surrounding level ice regions. Quantitative estimates of the surge force on the ice ridge due to the wave action are presented. The surge force is important for evaluating the motion of the ice ridge, and the bending moment is important for evaluating its tendency to break up. The thickness of level ice is ignored by assuming that the ridge draft is much thicker than the level ice.

## 2. Mathematical formulation

The analysis is performed in the three-dimensional cylindrical polar coordinate system  $(r, \theta, z)$  shown in Fig. 1 in water of finite depth  $h$  under the assumption of small amplitude waves. The ice ridge is modeled as a thin plate of radius  $a$  and draft  $d$ . As shown in the figure, the ridge axis is situated at  $r = 0$ , and the  $z$ -axis points directly upward with  $z = 0$  being the actual wetted ice covered surface. The notations  $I_s$  and  $I_g$  represent the submerged portion of the ice ridge and the gap between ice ridge and flat bottom respectively. The fluid is treated as inviscid and incompressible. The linearized governing equation and boundary conditions for the potential  $\Phi(r, \theta, z, t)$  are as follows:

$$\nabla^2 \Phi = 0 \quad -h < z < 0, \quad (1a)$$

$$\frac{\partial \Phi}{\partial z} = 0 \quad z = -h, \quad (1b)$$

$$\frac{\partial \Phi}{\partial z} = \frac{\partial \eta_j}{\partial t} \quad z = s_j, \quad (1c)$$

$$\rho \left( g \frac{\partial \Phi}{\partial z} + \frac{\partial^2 \Phi}{\partial t^2} \right) = -\frac{\partial p_j}{\partial t} \quad z = s_j, \quad (1d)$$

where  $j = 1$  represents the level ice, ( $r > a$ ), and  $j = 2$  the ice ridge, ( $r < a$ ), with  $s_1 = 0$  and  $s_2 = -d$ . In Eq. (1),  $\eta_j$  is the deflection,  $p_j$  is the pressure,  $\rho$  is the water density and  $g$  is the acceleration due to gravity. The radiation condition is applied at  $r \rightarrow \infty$ . The plate deflection  $\eta_j$  satisfies the Euler–Bernoulli thin plate equation:

$$D_j \nabla^4 \eta_j + \rho_j d_j \frac{\partial^2 \eta_j}{\partial t^2} = p_j \quad z = s_j, \quad (2)$$

where  $d_j, \rho_j$  are the thickness and density of domain  $j$  and  $D_j = E_j d_j^3 / 12(1 - \nu^2)$  with  $E_j$  and  $\nu$  are its Young's modulus and Poisson's ratio respectively.

Using Eqs. (1c) and (1d) in Eq. (2), the boundary condition beneath the  $j^{\text{th}}$  plate can be written as

$$D_j \nabla^4 \frac{\partial \Phi}{\partial z} + \rho_j d_j \frac{\partial}{\partial t^2} \frac{\partial \Phi}{\partial z} = -\rho \left( g \frac{\partial \Phi}{\partial z} + \frac{\partial^2 \Phi}{\partial t^2} \right) \quad z = s_j. \quad (3)$$

We adopt the following dimensionless form of the various quantities as in Meylan (2002).

$$\bar{r} = r/L, \quad \bar{z} = z/L, \quad \bar{\eta}_j = \eta_j/L, \quad \bar{t} = t\sqrt{g/L} \quad \text{and} \quad \bar{\Phi} = \Phi/(L\sqrt{Lg}),$$

with  $L$  being the characteristic length parameter, chosen as the wave amplitude. With progressive waves, the velocity potential can be expressed as  $\bar{\Phi}(\bar{r}, \bar{z}, \bar{t}) = \text{Re} \left\{ \bar{\phi}(\bar{r}, \bar{z}) e^{-i\bar{t}\sqrt{\alpha}} \right\}$  where the time-harmonic angular frequency  $\omega = \sqrt{\alpha}$ . Now, dropping the over bars for convenience, the boundary value problem can be expressed as the following:

$$\nabla^2 \phi = 0 \quad -h < z < 0, \quad (4a)$$

$$\frac{\partial \phi}{\partial z} = 0 \quad z = -h, \quad (4b)$$

$$\frac{\partial \phi}{\partial r} = 0 \quad -d < z < 0, \quad (4c)$$

$$(\beta_1 \nabla^4 + 1 - \alpha \gamma_1) \frac{\partial \phi}{\partial z} = \alpha \phi \quad r > a, z = 0, (4d)$$

$$(\beta_2 \nabla^4 + 1 - \alpha \gamma_2) \frac{\partial \phi}{\partial z} = \alpha \phi \quad r < a, z = -d, (4e)$$

with  $\beta_j = D_j / (\rho g L^4)$  and  $\gamma_j = \rho_j d_j / (\rho L)$  representing the dimensionless stiffness and mass, respectively. The radiation boundary condition is given by

$$\lim_{r \rightarrow \infty} \sqrt{r} \left( \frac{\partial}{\partial r} - i\alpha \right) (\phi - \phi_I) = 0. (5)$$

where  $\phi_I$  is the velocity potential of the incident wave, which can be written as

$$\phi_I = \frac{1}{i\sqrt{\alpha}} \sum_{m=0}^{\infty} I_m(k_0 r) f_0(z) \cos m\theta, (6)$$

with  $I_m$  being the modified Bessel function of the first kind of order  $m$ . Following Zilman and Miloh (2000), the connection between the ice ridge at  $r = a$  and ice cover satisfies the following conditions at  $z = -d$  and  $z = 0$  respectively when the ice ridge is free to move independently.

$$\left[ \bar{\Delta} - \frac{1-\nu}{r} \left( \frac{\partial}{\partial r} + \frac{1}{r} \frac{\partial^2}{\partial \theta^2} \right) \right] \eta_j = 0, (7a)$$

$$\left[ \frac{\partial}{\partial r} \bar{\Delta} - \frac{1-\nu}{r^2} \left( \frac{\partial}{\partial r} - \frac{1}{r} \frac{\partial^2}{\partial \theta^2} \right) \right] \eta_j = 0, (7b)$$

with  $\eta_j$  being the time-independent deflection of the domain  $j$ . However, when the ice ridge and level ice are frozen or welded together, the continuity of deflections, bending moments and shear forces along the edges yield the following conditions instead

$$\eta_1(r, \theta, 0) - \eta_2(r, \theta, -d) = 0, (8a)$$

$$\frac{\partial}{\partial r} \{ \eta_1(r, \theta, 0) - \eta_2(r, \theta, -d) \} = 0, (8b)$$

$$\left[ \bar{\Delta} - \frac{1-\nu}{r} \left( \frac{\partial}{\partial r} + \frac{1}{r} \frac{\partial^2}{\partial \theta^2} \right) \right] \{ \eta_1(r, \theta, 0) - \eta_2(r, \theta, -d) \} = 0, (8c)$$

$$\left[ \frac{\partial}{\partial r} \bar{\Delta} - \frac{1-\nu}{r^2} \left( \frac{\partial}{\partial r} - \frac{1}{r} \frac{\partial^2}{\partial \theta^2} \right) \right] \{ \eta_1(r, \theta, 0) - \eta_2(r, \theta, -d) \} = 0. (8d)$$

where  $\bar{\Delta} = \frac{\partial^2}{\partial r^2} + \frac{1}{r} \frac{\partial}{\partial r} + \frac{1}{r^2} \frac{\partial^2}{\partial \theta^2}$ . Finally, the respective continuity of normal velocity and pressure at the interface  $r = a$  along the gap yields

$$\left. \frac{\partial \phi}{\partial r} \right|_{r=a^+} = \left. \frac{\partial \phi}{\partial r} \right|_{r=a^-} \quad \text{and} \quad \phi|_{r=a^+} = \phi|_{r=a^-} \quad z \in I_g. \quad (9)$$

### 3. Solution method

Using the Fourier-Bessel series expansion, the velocity potential can be expanded in the following form

$$\phi(r, \theta, z) = \begin{cases} \sum_{m=0}^{\infty} \sum_{n=-2}^{\infty} A_{mn} K_m(k_n r) f_n(z) \cos m\theta & r > a, \\ \sum_{m=0}^{\infty} \sum_{n=-2}^{\infty} B_{mn} I_m(l_n r) g_n(z) \cos m\theta & r < a. \end{cases} \quad (10)$$

In the above,  $K_m$  is the modified Bessel function of the second kind of order  $m$ .  $k_n$  and  $l_n$  satisfy the dispersion relation  $\alpha + (\beta_1 k^4 + 1 - \alpha \gamma_1) k \tan kh = 0$  and  $\alpha + (\beta_2 l^4 + 1 - \alpha \gamma_2) l \tan l(h-d) = 0$ , respectively. The two relationships have one positive imaginary root  $k_0$  and  $l_0$ , respectively, two fully complex roots with a positive imaginary part  $\{k_{-2}, k_{-1}(=k_{-2}^*) \text{ and } l_{-2}, l_{-1}(=l_{-2}^*)\}$  where ‘\*’ denotes the complex conjugate, and infinitely many positive roots (see Fox and Squire (1994)). In Eq. (10),  $f_n(z) = \cos k_n(z+h) / \cos k_n h$  and  $g_n(z) = \cos l_n(z+h) / \cos l_n h$  are the eigenfunctions.

The boundary conditions and edge conditions are now applied to the surface of the ice ridge and the gap separately. From the ice ridge boundary condition Eq. (4c), using the expression for  $\phi$  from Eq. (10) and the orthogonal properties of  $\cos m\theta$  over the interval  $0 \leq \theta \leq 2\pi$ , it is derived that

$$\sum_{n=-2}^{\infty} A_{mn} k_n K'_m(k_n a) f_n(z) + \frac{k_0}{i\sqrt{\alpha}} I'_m(k_0 a) f_0(z) = 0 \quad z \in I_s. \quad (11)$$

For the gap region, using the orthogonality of  $\cos m\theta$  over the interval  $0 \leq \theta \leq 2\pi$  and with the continuity of pressure and velocity along the gap as shown in Eq. (9), yields

$$\sum_{n=-2}^{\infty} A_{mn} K_m(k_n a) f_n(z) - \sum_{n=-2}^{\infty} B_{mn} I_m(l_n a) g_n(z) + \frac{1}{i\sqrt{\alpha}} I_m(k_0 a) f_0(z) = 0 \quad z \in I_g. \quad (12)$$

$$\sum_{n=-2}^{\infty} A_{mn} k_n K'_m(k_n a) f_n(z) - \sum_{n=-2}^{\infty} B_{mn} l_n I'_m(l_n a) g_n(z) + \frac{k_0}{i\sqrt{\alpha}} I'_m(k_0 a) f_0(z) = 0 \quad z \in I_g, \quad (13)$$

As discussed above, two approaches are adopted in this study to reduce the dual series relations to a system of algebraic equations. In the first approach, we obtain a closed form solution using the inner product of the vertical eigenfunctions associated with the ice covered region without considering the effect of submergence. The same approach was used in Peter et al. (2004) to analyse the wave induced response of a circular elastic plate in open water. In the second approach, we use the least square approximation method to include the effect of submergence of the ice ridge.

### 3.1. Approach I: Closed form solution

In this subsection, a closed form solution is obtained assuming that the circular ice ridge is thin and has a shallow draft with  $d = 0$ . The orthogonal mode-coupling relation for the plate covered region can be written as the following (see Manam et al. (2006))

$$\begin{aligned} \langle h_{mn}(\theta, z), h_{pq}(\theta, z) \rangle &= \int_{2\pi}^0 \left\{ \int_{-h}^0 h_{mn}(\theta, z) h_{pq}(\theta, z) dz \right. \\ &\quad \left. + \frac{\beta_j}{\alpha} \left( h'_{mn}(\theta, 0) h'''_{pq}(\theta, 0) + h'''_{mn}(\theta, 0) h'_{pq}(\theta, 0) \right) \right\} d\theta = G(r_n) \delta_{mp} \delta_{nq}, \end{aligned} \quad (14)$$

where  $\delta_{mp}$  and  $\delta_{nq}$  are the Kronecker delta, and the primes are denoting the derivative with respect to  $z$ . For  $r < a$ ,  $h_m, h_n = f_m, f_n$ ;  $G(r_n) = G(k_n)$  and for  $r > a$ ,  $h_m, h_n = g_m, g_n$ ;  $G(r_n) = G(l_n)$  with  $G(r_n) = -\frac{8r_n^5 \beta_j \sin^2 r_n h - \alpha (2r_n h + \sin 2r_n h)}{4r_n \alpha \cos^2 r_n h}$ .

It is important to note that  $\beta_j = 0$  yields the form of the orthogonal relation satisfied by the open water region eigenfunctions. Hence,  $\beta_1 = 0$  reproduces the solution of Peter et al. (2004). For later reference, we note that

$$\int_{-h}^0 f_m(z) g_n(z) dz = H(k_m, l_n) \quad \text{where} \quad H(k_m, l_n) = \frac{k_m \sin k_m h \cos l_n h - l_n \sin l_n h \cos k_m h}{(k_m^2 - l_n^2) \cos k_m h \cos l_n h},$$

with  $I_s = 0$  and  $I_g = (-d, 0)$ . Hence, applying the orthogonal mode-coupling relation for the ice cover region as defined in Eq. (14) in the algebraic Equations (12)-(13) yields

$$\frac{\delta_{0s}}{i\sqrt{\alpha}} I_m(k_0 a) G(k_0) + A_{ms} K_m(k_s a) G(k_s) = \sum_{n=-2}^{\infty} B_{mn} I_m(l_n a) H(k_s, l_n) + k_s \frac{\beta_1}{\alpha} (\kappa_m k_s^2 - \tau_m) \tan k_s h, \quad (15a)$$

$$\frac{\delta_{0s} k_0}{i\sqrt{\alpha}} I'_m(k_0 a) G(k_0) + A_{ms} k_s K'_m(k_s a) G(k_s) = \sum_{n=-2}^{\infty} B_{mn} l_n I'_m(l_n a) H(k_s, l_n) + k_s \frac{\beta_1}{\alpha} (\tilde{\kappa}_m k_s^2 - \tilde{\tau}_m) \tan k_s h, \quad (15b)$$

where  $\kappa_m, \tau_m, \tilde{\kappa}_m$  and  $\tilde{\tau}_m$  are given by:

$$\phi_{I_z}(a, \theta, 0) + \phi_z(a, \theta, 0) = \sum_{m=0}^{\infty} \kappa_m \cos m\theta, \quad \phi_{I_{zzz}}(a, \theta, 0) + \phi_{zzz}(a, \theta, 0) = \sum_{m=0}^{\infty} \tau_m \cos m\theta, \quad (16a)$$

$$\phi'_{I_z}(a, \theta, 0) + \phi'_z(a, \theta, 0) = \sum_{m=0}^{\infty} \tilde{\kappa}_m \cos m\theta, \quad \phi'_{I_{zzz}}(a, \theta, 0) + \phi'_{zzz}(a, \theta, 0) = \sum_{m=0}^{\infty} \tilde{\tau}_m \cos m\theta, \quad (16b)$$

with prime denoting the derivative with respect to  $r$  and subscript  $z$  denotes the derivative with respect to  $z$ . Now we set the upper limit in the summations of  $n$  as  $N$  and of  $m$  as  $M$  in Eqs. (15)-(16), respectively. This leads to a system of  $2N+6$  equations with  $2N+10$  unknowns. Hence, four extra equations are required which can be obtained from the edge conditions in Eq. (7) or (8).

### 3.2. Approach II: Least Square Approximation Method (LSAM)

LSAM was initially developed by Kelman and Koper (1973) to approximate the solutions of general dual trigonometric equations, and its convergence for square integrable functions has been studied theoretically by Feinerman et al. (1974). Subsequently, LSAM is used to deal with wave scattering by partial barriers successfully (see Lee et al. (2000)). In this study, the ice ridge's submergence effect is considered ( $d > 0$ ). Hence Approach I can not be used to obtain a matrix system using the orthogonal properties of vertical eigen functions.

The series relationships defined over  $I_s$  and  $I_g$ , in Eqs. (11), (12) and (11), (13) produce two sets of dual series relations defined over the range  $I_s \cup I_g$ . These dual series relations can be rewritten in the following form

$$F(z) = \sum_{n=-2}^{\infty} A_{mn} V_{a_n}(z) + \sum_{n=-2}^{\infty} B_{mn} V_{b_n}(z) + V_0(z) = 0. \quad (17)$$

Hence, truncating the first infinite series after  $N+3$  terms and second infinite series after  $N+7$  terms, the truncated series  $F_N(z)$  of  $F(z)$  is defined as

$$F_N(z) = \sum_{n=-2}^N A_{mn} V_{a_n}(z) + \sum_{n=-2}^{N+4} B_{mn} V_{b_n}(z) + V_0(z), \quad (18)$$

where  $V_{a_n}(z), V_{b_n}(z)$  and  $V_0(z)$  can be chosen in an appropriate manner for specific dual series relations subsequently. Since  $F(z) = 0$ , using LSAM, it is derived that

$$\int_{I_s \cup I_g} |F_N(z)|^2 dz = \text{minimum}. \quad (19)$$



Minimizing the above integral in Eq. (19) with respect to  $A_{mn}$  yields

$$\int_{I_s \cup I_g} F_N^*(z) \frac{\partial F_N(z)}{\partial A_{mn}} dz = 0. \quad (20)$$

where ‘\*’ denotes the complex conjugate. Substituting Eq. (11) and Eq. (13) into Eq. (20), the following system of equations is obtained.

$$\sum_{n=-2}^N A_{mn}^* P_{nl} + \sum_{n=-2}^{N+4} B_{mn}^* Q_{nl} = b_{ml}, \quad (l = -2, -1, 0, \dots, N), \quad (21)$$

with

$$P_{nl} = \int_{I_s} W_{a_{mn}}^*(z) W_{a_{ml}}(z) dz + \int_{I_g} Y_{a_{mn}}^*(z) Y_{a_{ml}}(z) dz, \quad Q_{nl} = \int_{I_g} Y_{b_{mn}}^*(z) Y_{a_{ml}}(z) dz,$$

$$b_{ml} = -\int_{I_s} W_m^*(z) W_{a_{ml}}(z) dz + \int_{I_g} Y_m^*(z) Y_{a_{ml}}(z) dz,$$

where  $W_{a_{mn}}(z) = k_n K'_m(k_n a) f_n(z)$ ,  $Y_{a_{mn}}(z) = k_n K'_m(k_n a) f_n(z)$ ,  $Y_{b_{mn}}(z) = -l_n I'_m(l_n a) g_n(z)$ ,  $W_m(z) =$

$$\frac{k_0}{i\sqrt{\alpha}} I'_m(k_0 a) f_0(z) \quad \text{and} \quad Y_m(z) = \frac{k_0}{i\sqrt{\alpha}} I'_m(k_0 a) f_0(z).$$

In a similar way, using Eq. (11) and Eq. (12) and minimizing the integral in Eq. (19) with respect to  $A_{mn}$ , another system of equations can be obtained. Together, the two systems of equations give  $2N + 6$  equations which contain  $2N + 10$  unknowns. The remaining equations come from the edge conditions as shown in Eq. (7) or (8). It should be noted that the substitution of  $d = 0$  in the present approach yields the same results obtained from Approach I. However, LSAM is more general compared to the Approach I.

### 3.3. Special cases

Some special cases of the present problem can be readily studied as listed below.

(a) *A continuous ice cover with a circular crack*

In case of a continuous ice cover with a circular crack, the analysis can be presented using Approach I by setting  $\beta_1 = \beta_2$  and  $\gamma_1 = \gamma_2$ .

(b) *A truncated rigid cylinder embedded in ice cover*

In case of a truncated rigid cylinder of draft  $d$ ,  $I_g = -h < z < -d$  and  $I_s = -d < z < 0$  and  $\beta_2 = \infty$ .

Approach II can be used, and the unknown coefficients can be obtained.

(c) *A complete rigid cylinder embedded in ice cover*

In case of a rigid cylinder extending from the free surface to the bottom,  $I_g = 0$  and  $I_s = -h < z < 0$ , hence  $d = -h$ . The velocity potential exists only in the region  $r > a$  in Eq. (10). Using the orthogonal mode-coupling relation for the ice covered region, Eqs. (15a)-(15b) reduce to the following:

$$\frac{\delta_{0s}}{i\sqrt{\alpha}} I_m(k_0 a) G(k_0) + A_{ms} K_m(k_s a) G(k_s) = k_s \frac{\beta_1}{\alpha} (\kappa_m k_s^2 - \tau_m) \tan k_s h, \quad (22)$$

$$\frac{\delta_{0s} k_0}{i\sqrt{\alpha}} I'_m(k_0 a) G(k_0) + A_{ms} k_s K'_m(k_s a) G(k_s) = k_s \frac{\beta_1}{\alpha} (\tilde{\kappa}_m k_s^2 - \tilde{\tau}_m) \tan k_s h. \quad (23)$$

Thus, in a similar way as in Approach I, the complex coefficients associated with the scattered potentials can be obtained.

Cases (b) and (c) can be compared with Garrett (1971) and Niedzwecki and Duggal (1992), respectively, where a circular cylinder surrounded by open water was studied. The present study focuses on (a) and its extension to finite draft deformable inclusion either free or frozen to its surrounding level ice.

#### 4. Deflection, surge force, and bending moment

After the velocity potentials are obtained, the response of the ice ridge to various wave and ridge parameters may be calculated.

Using Eqs. (4d) and (4e) with the kinematic boundary condition in their appropriate region, the deflection can be expressed as

$$\eta(r, \theta) = \begin{cases} \sum_{m=0}^{\infty} \sum_{n=-2}^{\infty} i\sqrt{\alpha} (\beta_1 k_n^4 + 1 - \alpha\gamma_1)^{-1} A_{nm} K_m(k_n r) \cos m\theta & r > a, \\ \sum_{m=0}^{\infty} \sum_{n=-2}^{\infty} i\sqrt{\alpha} (\beta_2 l_n^4 + 1 - \alpha\gamma_2)^{-1} B_{nm} I_m(l_n r) g_n(-d) \cos m\theta & r \leq a. \end{cases} \quad (24)$$

The surge force is calculated by integrating the fluid pressure around the vertical surface of the ridge.

$$\begin{aligned} f_s &= a \int_0^{2\pi} \int_{-d}^0 p_1 \cos(\pi - \theta) dz d\theta \\ &= -i\rho a L g \sqrt{\alpha} \sum_{m=0}^{\infty} \int_0^{2\pi} \left[ \frac{I_m(k_0 a)}{i\sqrt{\alpha}} \int_{-d}^0 f_0(z) dz + \sum_{n=-2}^{\infty} A_{nm} K_m(k_n a) \int_{-d}^0 f_n(z) dz \right] \cos m\theta \cos \theta d\theta. \end{aligned} \quad (25)$$

In Eq. (25), it is observed that after applying the orthogonality of  $\cos m\theta$  over the interval

$0 \leq \theta \leq 2\pi$ , the surge excitation force only becomes nonzero if  $m = 1$ . Hence,

$$f_s = -i2\pi\rho a L g \sqrt{\alpha} \left( \frac{s_0}{i\sqrt{\alpha}} I_1(k_0 a) + \sum_{n=-2}^{\infty} s_n A_{1n} K_1(k_n a) \right) \text{ with } s_n = \frac{\sin k_n h - \sin k_n (h-d)}{k_n \cos k_n h}. \quad (26)$$

The bending moment distribution of the ice ridge is important to determine whether an ice floe may break under the wave action. Following Zilman and Miloh (2000), the bending moment at  $(r, \theta, -d)$  can be written as

$$M_{r,\theta} = \left[ \bar{\Delta} - \frac{1-\nu}{r} \left( \frac{\partial}{\partial r} + \frac{1}{r} \frac{\partial^2}{\partial \theta^2} \right) \right] \eta_2 \quad r \leq a, z = -d. \quad (27)$$

Using Eq. (24), Eq. (27) can be rewritten as follow:

$$M_{r,\theta} = \sum_{m=0}^{\infty} \sum_{n=-2}^{\infty} \frac{i\sqrt{\alpha} g_n(-d)}{(\beta_2 l_n^4 + 1 - \alpha \gamma_2)} B_{mn} \left( l_n^2 I_m(l_n r) - \frac{1-\nu}{r} \left( l_n I_m'(l_n r) - \frac{m^2}{r} I_m(l_n r) \right) \right) \cos m\theta \quad r \leq a. \quad (28)$$

It is important to note that Eq. (28) is undefined at the origin. Using the asymptotic behavior of Bessel functions for small arguments (see Abramowitz and Stegun (1970)), it can be approximated that

$$M_{r,\theta} \sim \sum_{n=-2}^{\infty} \frac{i\sqrt{\alpha} g_n(-d)}{4(\beta_2 l_n^4 + 1 - \alpha \gamma_2)} \left( 2B_{0n} l_n^2 (1+\nu) + B_{2n} l_n^2 (1-\nu) \cos 2\theta \right) \quad r \sim 0. \quad (29)$$

The location of maximum bending moment is where the ridge is most likely to break under the wave action. The modulus of the bending moment and maximum bending moment are denoted by  $M_B$  and  $M_{B_{\max}}$  respectively.

## 5. Numerical results

Based on the above solutions, several typical cases are analyzed below with  $L = 1\text{m}$ . The physical and mechanical properties of sea ice and ice ridge are extracted from Untersteiner (1986), Peter et al. (2004) and Ekeberg (2015). The Young's modulus of the ice ridge is fixed at 3GPa except when studying its effect. The density of both ice types is assumed to be the same at  $922.5 \text{ kg/m}^3$ , while the water density is  $1025 \text{ kg/m}^3$ . The dimensionless ice ridge radius is set at  $a = 100$ , wavelength 50, Poisson ratio  $\nu = 0.3$  and water depth  $h = 25$ .  $\gamma_j = 0$  when submergence effect of the ridge is neglected otherwise  $\gamma_j = \rho_j d_j / (\rho L)$ . These values are fixed for all examples unless otherwise stated. Using the formulae derived in the previous section, we can compute the amplitude of deflections and surge excitation force on the ice ridge.

In Fig.2, we reproduce the results in Peter et al. (2004) by setting  $\beta_1 = 0$  and  $\gamma_1 = 0$ , thus validating the present approach. The convergence of the solution depends on the geometry and the flexural rigidity of the ice ridge. For computational purpose, we truncate after  $M = 8$ , taking into account the convergence of various series in the system of equations. In addition,  $N$  is restricted to 8 which is similar to that of Peter et al. (2004). It is important to note that the use of LSAM is preferred compared to the closedform solution approach, since LSAM can handle the ice ridge's submergence effect.

With the above validation, we proceed to examine some special cases. Fig. 3 represents the case when the ice ridge is embedded in an ice cover of the same draft. In this case, both approaches produce the same result. In Fig. 3(a), the amplitude of ice ridge deflection is computed with the free edge conditions while in Fig. 3(b), the ice ridge and level ice are frozen together. The results show that the deflection is much smaller compared to the case of open water in Fig. 2. The case in Fig. 3(a) can be considered as a circular crack, since the level ice and ice ridge have identical properties. If they are frozen together, we expect that the wave pattern should be identical to a plane wave propagating underneath continuous level ice. Fig. 3(b) is indeed very close to this situation.

We now examine effects of ridge parameters and wave properties in the ridge response. In Figs.4 - 10, various values of  $E$  and  $d$  are used for  $\beta_2 = Ed^3 / \{12(1-\nu^2)\rho gL^4\}$ . We set  $\beta_1 = 0$  for open water cases and  $\beta_1 = 10^4$  in the presence of level ice.

Fig. 4 compares the results with and without the draft consideration for the ice ridge in open water ( $\beta_1 = 0$ ). It is evident from the figure that with the smallest draft ( $d = 0.05h$ ), the solutions are similar to Fig.2, and there is no difference between the two solution approaches. As the ice ridge draft increases, the effect of submergence becomes more pronounced and the deflection patterns are now different between them.

In Fig.5, it can be observed that as the ice ridge flexural rigidity increases, the deflection decreases and the ridge acts more like a rigid structure. The same happens when the ridge thickness is increased.

In Fig.6, as the ridge radius increases, the number of crests and troughs increases. The figure thus depicts that the ice ridge radius may influence the attributes of the flexure for a fixed draft. However, certain peaks in the ice ridge deflection are observed with an increase in ridge radius which are due to the mutual interaction of gravity waves with various spatial modes of ridge vibration. When the diameter of ice ridge becomes greater than the incoming wavelength, the ridge is subjected to multiple wave cycles spatially. Ridge breakup can occur under this resonance. From Figs.5 - 6, it can be observed that not only the radius but also the draft contributes to the flexure of the ice ridge.

To better investigate the deflection pattern within the ice ridge, mesh plots and contour plots are provided in Fig.7. It can be observed that the deflection of the ice ridge is larger when surrounded by open water than by level ice. A comparison between Figs.7(c,d) and 7(e,f) reveals that the presence of a circular crack significantly affects the deflection pattern.

For practical applications, when an ice cover becomes mobile, the embedded ridges are more likely already detached from the surrounding level ice cover. Hence in the next set of calculations, we focus on the free edge case only.

To investigate the wave induced forces on the ice ridge, Fig.8 shows the dimensionless surge force in the presence of a level ice with the free edge condition. The dimensionless surge force on the ice ridge is defined as  $F_s = \left| f_s / (\rho g a d^2) \right|$  where  $f_s$  is the surge excitation force as in Eq. (26). In Fig. 8, the dimensionless surge forces are plotted versus the dimensionless incident wave number  $k_0 a$  for various ice ridge drafts. Since the dynamic pressure decreases with depth, even though the dimensional surge force increases with the ridge draft, the dimensionless force does not. As discussed before, an increasing ridge draft translates to an increasing flexure rigidity parameter  $\beta_2$ . In this case, where the edge of the ice ridge is free, the maximum surge force does not change much between the case of an ice ridge surrounded by open water or level ice, but the actual surge force under different impinging waves do differ between these two cases. The general trend of the surge force drops with an increase in the wave number. Furthermore, the surge force vanishes for certain values of ridge draft, which is due to the destructive interference of the incoming and scattered waves.

In Fig. 8, the dimensionless surge forces are plotted versus the dimensionless  $k_0 h$ . Both figures reveal that the maximum dimensionless surge force is almost independent of  $a/d$ . Hence the maximum dimensional surge force is mainly dependent on  $h/d$ . It is also observed that the level ice significantly affects the ice ridge response to shorter waves.

To study the tendency for an ice ridge to fracture due to wave actions, the bending moments are plotted in Figs.9 – 10, for an ice ridge surrounding by open water and level ice respectively. The variations of the bending moment modulus  $M_B$  over the ice ridge are shown by contour plot in Fig. 9. In Fig.10, the maximum bending moments are plotted versus the dimensionless wavelength  $\lambda/h$ . It is observed that the ridge embedded in the ice cover experiences larger  $M_{B_{\max}}$  compared to the open water case due to the larger spatial derivative of the deflection. With the increase of ridge flexural rigidity, the maximum bending moment decreases. The maxima in the figure are due to the constructive interference between the incident and reflected waves, while the minima correspond to

their destructive interference. The figure reveals that for larger wavelengths, the fluctuations of  $M_{Bmax}$  with respect to the wavelength decrease.

## 6. Discussion and Conclusions

In the present study, the response of the circular ice ridge with finite draft embedded in an ice sheet is analyzed mathematically. Two independent solution approaches, namely the closed form solution method and the least square approximation method, are adopted. The ice ridge deflection and surge force on the ridge are evaluated for various wave and ridge characteristics. The solutions are first validated with Peter et al. (2004) for the case of open water. Subsequently, the results show that the submergence of the ice ridge affects the ice ridge deflection in the presence of ice cover considerably. The presence of the surrounding level ice reduces the ice ridge deflection but increases the maximum bending moment. Hence, while intuitively the level ice offers a “protection” to the integrity of the ridge, its effect is mixed. With the presence of the level ice, the most significant effects are:

- The deflection of the ice ridge reduces but the bending moment increases when surrounded by (but detached from) level ice. The deflection is larger with a frozen edge than free edge.
- For fixed ridge draft and radius, the maximum surge force remains the same with or without the presence of the level ice, but the average surge force is affected, especially for shorter waves.

Both the ridge radius and incident wavelength are important factors affecting the ridge fracture. The results from the present study may be coupled with satellite remote sensing data to conduct a statistical analysis for the potential of ice ridge break up under incoming wave action. Given the dominant wavelength, ridge size and thickness, its rigidity and flexural strength, one may then estimate the breakup likelihood. Such statistical analysis can potentially produce useful information for polar ocean engineering applications.

## Acknowledgements

The authors gratefully acknowledge the funding provided by Ministry of Education, Singapore through the AcRF Tier 2 Grant No. MOE2013-T2-1-054. This work is supported in part by the US Office of Naval Research Global Grant No: N62909-15-1-2069. CSIR-NIO’s contribution No. xxxx.

## References

- Abramowitz, M and Stegun, I.A., 1970. Handbook of Mathematical Functions. Dover.
- Andrianov, A.I. and Hermans, A.J., 2005. Hydroelasticity of a circular plate on water of finite or infinite depth. Journal of Fluids and Structures, 20(5), 719-733.

- Andrianov, A.I. and Hermans, A.J., 2006. Hydroelastic analysis of a floating plate of finite draft. *Applied Ocean Research*, 28(5), 313-325.
- Bennetts, L.G., Biggs, N.R.T. and Porter, D., 2007. A multi-mode approximation to wave scattering by ice sheets of varying thickness. *Journal of Fluid Mechanics*, 579, 413-443.
- Bennetts, L.G. and Williams, T.D., 2010. Wave scattering by ice floes and polynyas of arbitrary shape. *Journal of Fluid Mechanics*, 662, 5-35.
- Finnegan, W., Meere, M. and Goggins, J., 2013. The wave excitation forces on a truncated vertical cylinder in water of infinite depth. *Journal of Fluids and Structures*, 40, 201-213.
- Garrett, C.J.R., 1971. Wave forces on a circular dock. *Journal of Fluid Mechanics*, 46(01), 129-139.
- Kvadsheim, S., 2014. Ice ridge keel size distributions. PhD Thesis.
- Linton, C.M. and McIver, P., 2001. *Handbook of mathematical techniques for wave/structure interactions*. CRC Press.
- Mandal, S., Datta, N. and Sahoo, T., 2013. Hydroelastic analysis of surface wave interaction with concentric porous and flexible cylinder systems. *Journal of Fluids and Structures*, 42, 437-455.
- Meylan, M.H. and Squire, V.A., 1996. Response of a circular ice floe to ocean waves. *Journal of Geophysical Research-All Series*, 101(C4), 8869-8884.
- Meylan, M.H., 2002. Wave response of an ice floe of arbitrary geometry. *Journal of Geophysical Research: Oceans*, 107(C1), 3005.doi:10.1029/2000JC000713.
- Mondal, R., Mandal, S. and Sahoo, T., 2014. Surface gravity wave interaction with circular flexible structures. *Ocean Engineering*, 88, 446-462.
- Montiel, F., Bonnefoy, F., Ferrant, P., Bennetts, L.G., Squire, V.A. and Marsault, P., 2013. Hydroelastic response of floating elastic discs to regular waves. Part 1. Wave basin experiments. *Journal of Fluid Mechanics*, 723, 604-628.
- Montiel, F. and Squire, V.A., 2015. Hydroelastic perspectives of ocean wave/sea ice connectivity II. 7th International Conference on Hydroelasticity in Marine Technology Split, Croatia.
- Niedzwecki, J.M. and Duggal, A.S., 1992. Wave runup and forces on cylinders in regular and random waves. *Journal of Waterway, Port, Coastal, and Ocean Engineering*, 118(6), 615-634.
- Peter, M.A., Meylan, M.H. and Chung, H., 2004. Wave scattering by a circular elastic plate in water of finite depth: a closed form solution. *International Journal of Offshore and Polar Engineering*, 14(02), 81-85.
- Squire, V.A., Dugan, J.P., Wadhams, P., Rottier, P.J. and Liu, A.K., 1995. Of ocean waves and sea ice. *Annual Review of Fluid Mechanics*, 27(1), 115-168.
- Squire, V. A., 1995. Engineering repercussions of ocean wave propagation in ice-infested seas, in *Proceedings of the 5th International Offshore and Polar Engineering Conference*, vol. 2, p. 1, Int. Soc. of Offshore and Polar Eng., Golden, Colo.

Squire, V.A. and Dixon, T.W., 2001. On modelling an iceberg embedded in shore-fast sea ice. *Journal of Engineering mathematics*, 40(3), 211-226.

Squire, V.A., 2007. Of ocean waves and sea-ice revisited. *Cold Regions Science and Technology*, 49(2), 110-133.

Tsubogo, T., 2001. The motion of an elastic disk floating on shallow water in waves. In *Proceeding of the Eleventh International Offshore and Polar Engineering Conference*. International Society of Offshore and Polar Engineers.

Williams, T.D. and Squire, V.A., 2008. The effect of submergence on wave scattering across a transition between two floating flexible plates. *Wave Motion*, 45(3), 361-379.

Williams, T.D. and Porter, R., 2009. The effect of submergence on the scattering by the interface between two semi-infinite sheets. *Journal of Fluids and Structures*, 25(5), 777-793.

Zilman, G. and Miloh, T., 2000. Hydroelastic buoyant circular plate in shallow water: a closed form solution. *Applied ocean research*, 22(4), 191-198.

### Figures and Captions

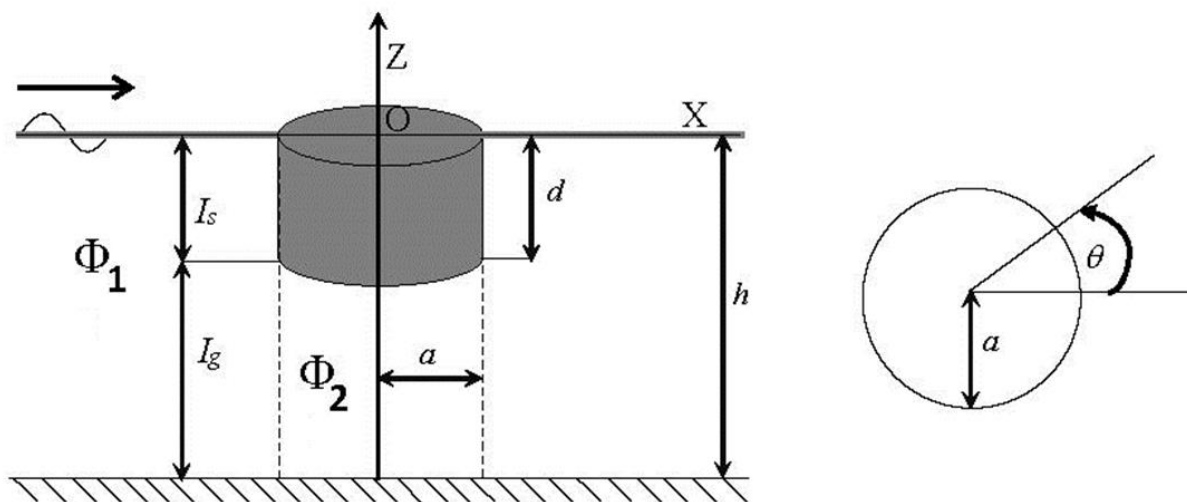


**Figure 1.** Schematic diagram for wave scattering by a circular ice ridge embedded in level ice.



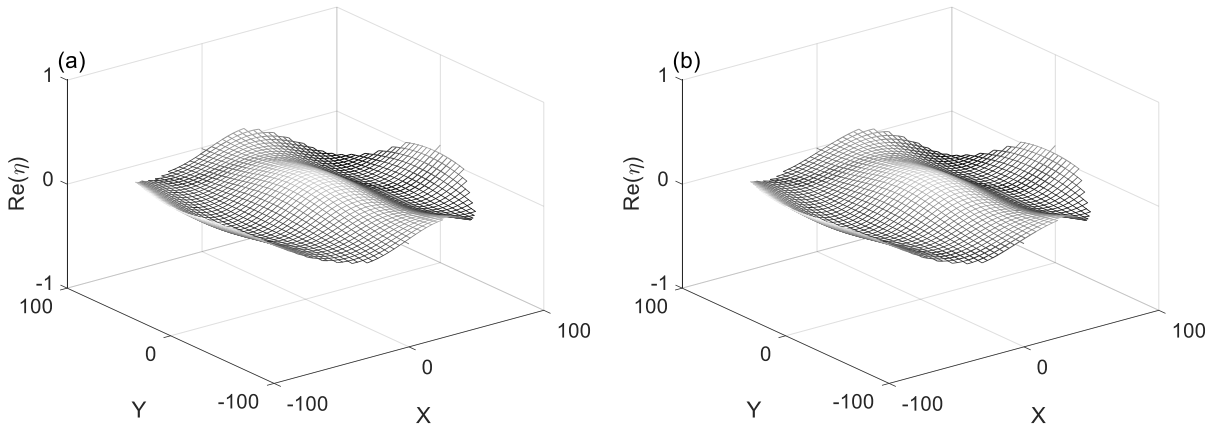


**Figure 2.** Ice ridge deflection in open water computed using (a) closed form solution and (b) LSAM with  $d = 0$ ,  $\beta_1 = 0$  and  $\beta_2 = 10^5$ .

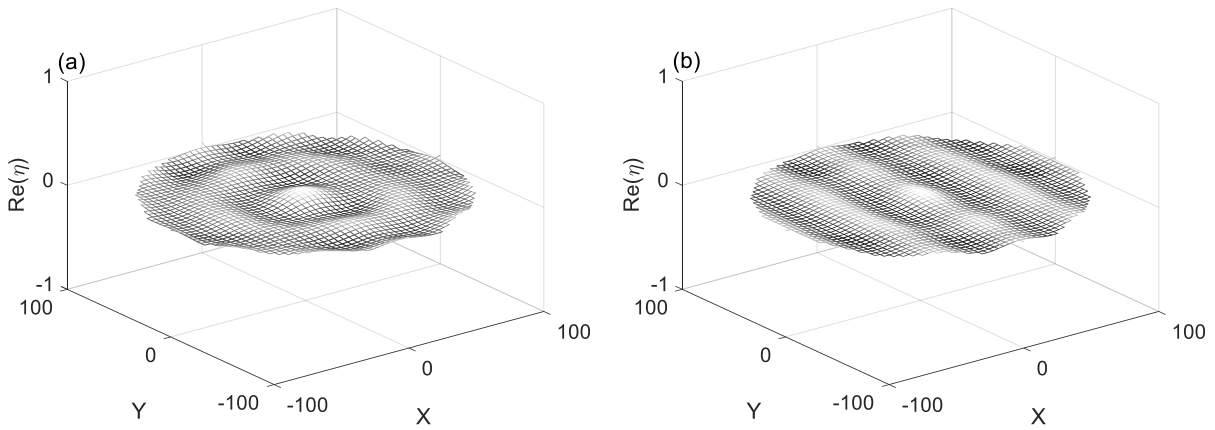


**Figure 3.** Ice ridge deflection with (a) free edge conditions and (b) fixed edge conditions with  $d = 0$ ,  $\beta_1 = \beta_2 = 10^5$ .

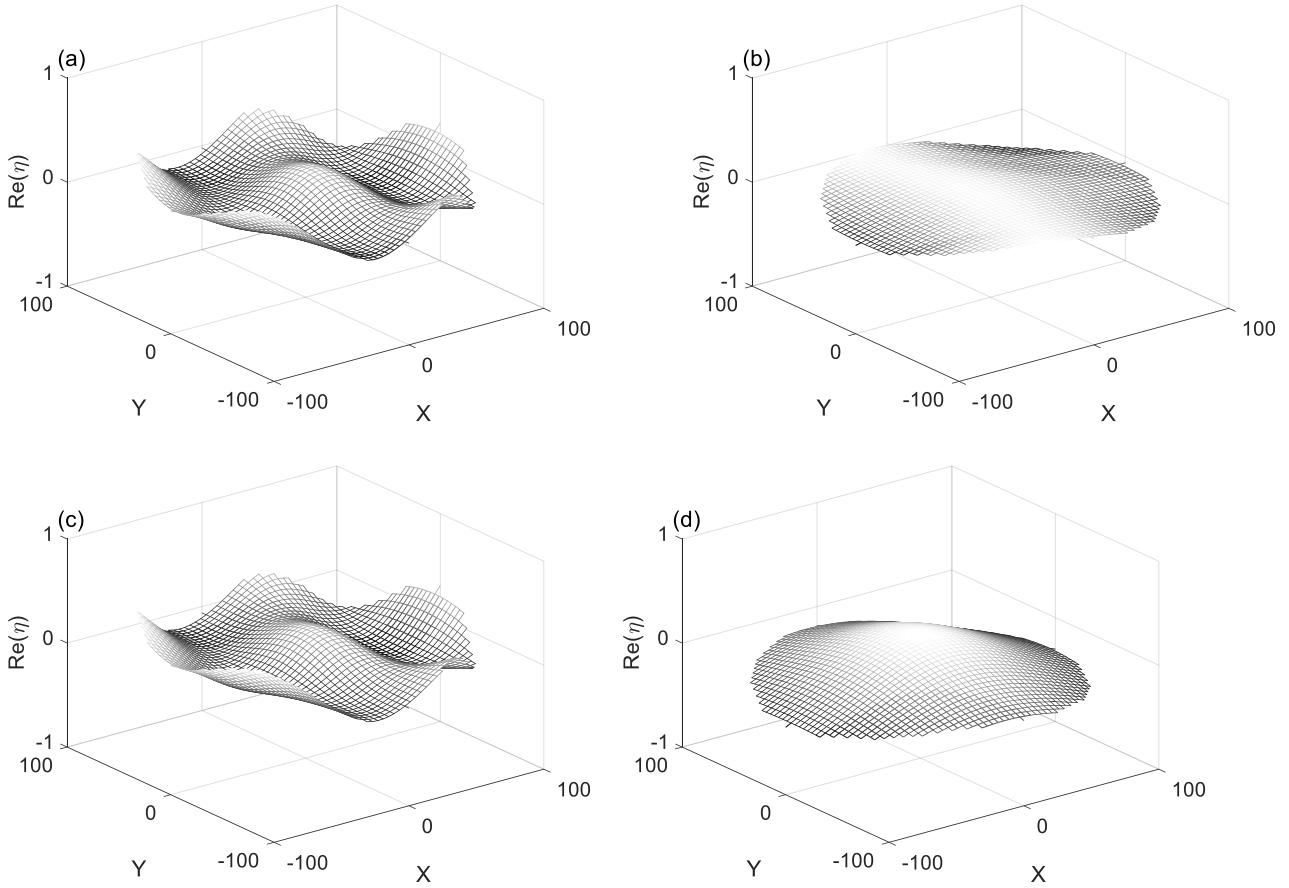


**Figure 4.** Iceridge deflection with  $\beta_1 = 0$  without draft consideration for (a)  $d = 0.05h, \beta_2 = 1.06 \times 10^5$  and (b)  $d = 0.15h, \beta_2 = 2.9 \times 10^6$  and with draft consideration for (c)  $d = 0.05h, \beta_2 = 1.06 \times 10^5$  and (d)  $d = 0.15h, \beta_2 = 2.9 \times 10^6$ .

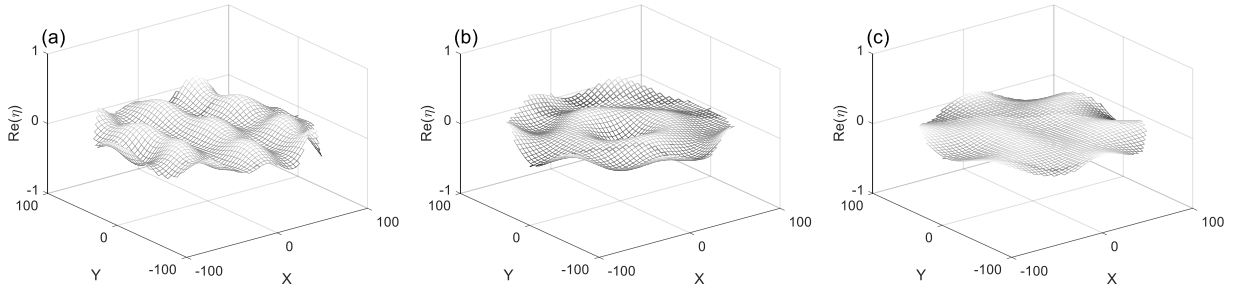


**Figure 5.** Ice ridge deflection for different ridge flexural rigidity for  $d = 0.05h$  with  $\beta_1 = 10^4$  and  $\beta_2 =$  (a)  $1.78 \times 10^4$  ( $E = 1\text{GPa}$ ), (b)  $5.34 \times 10^4$  ( $E = 3\text{GPa}$ ), and (c)  $1.06 \times 10^5$  ( $E = 6\text{GPa}$ ). Free edge condition is applied to the ice ridge.

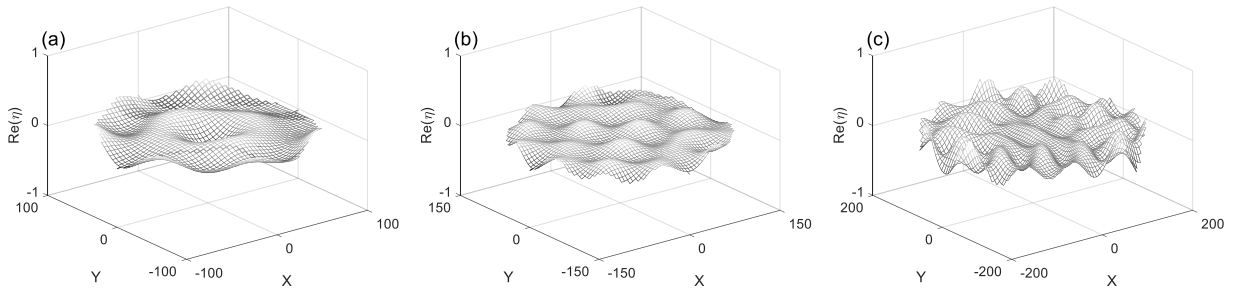


**Figure 6.** Ice ridge deflection for different ridge radius for  $d = 0.05h$  with  $\beta_1 = 10^4$ ,  $\beta_2 = 5.34 \times 10^4$  ( $E = 3\text{GPa}$ ) and (a)  $a = 4h$ , (b)  $a = 6h$ , and (c)  $a = 8h$ . Free edge condition is applied to the ice ridge.

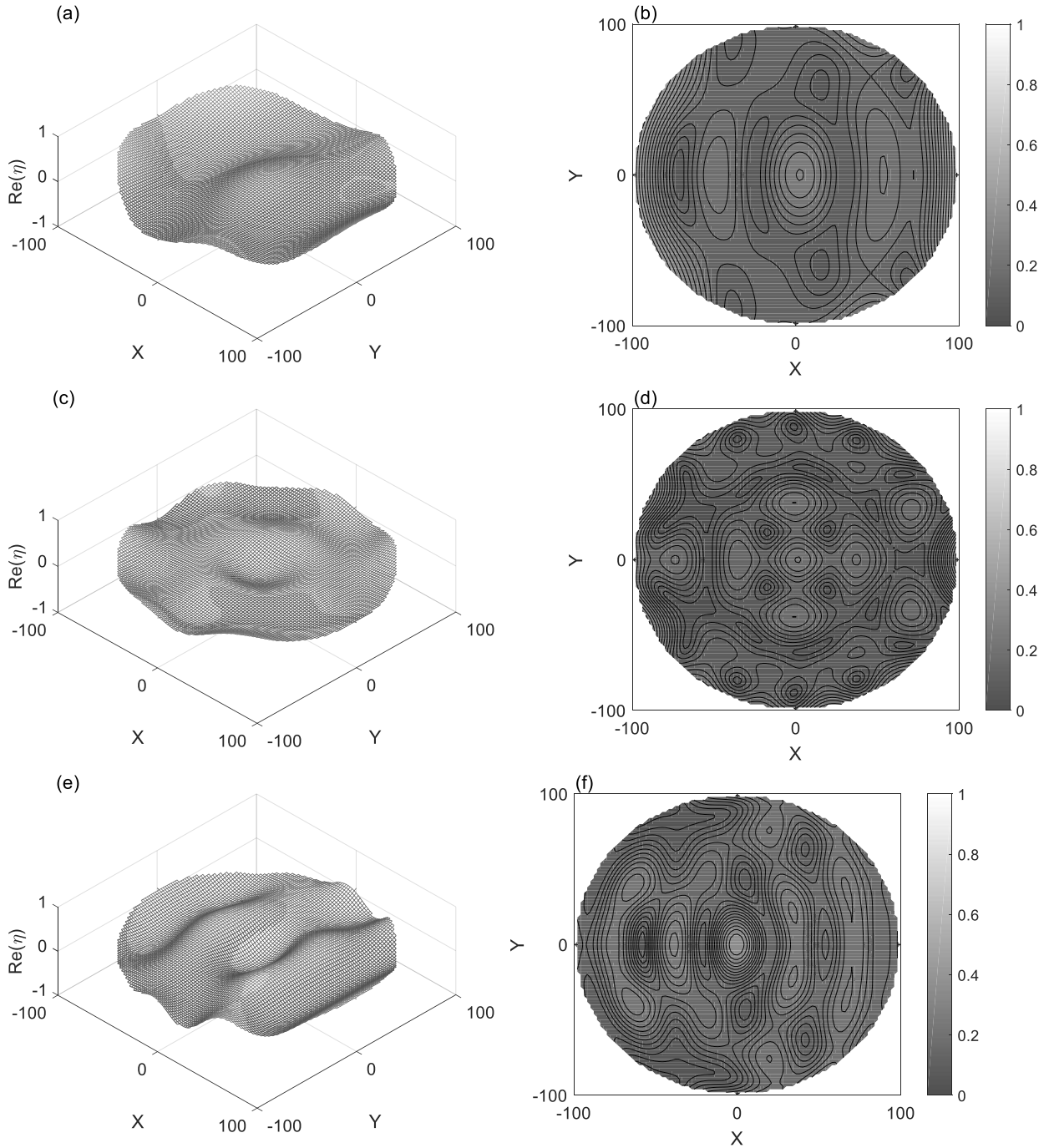


**Figure 7.** (a,c,e) Deflection; and (b,d,f) contour plot of the deflection with  $d = 0.05h$ . The first row is the results of an ice ridge in open water with  $\beta_1 = 0$  and the middle and last rows are results of the same ice ridge surrounded by level ice with  $\beta_1 = 10^4$ ,  $\beta_2 = 5.34 \times 10^4$  ( $E = 3$  GPa) having free edge and fixed edge respectively.

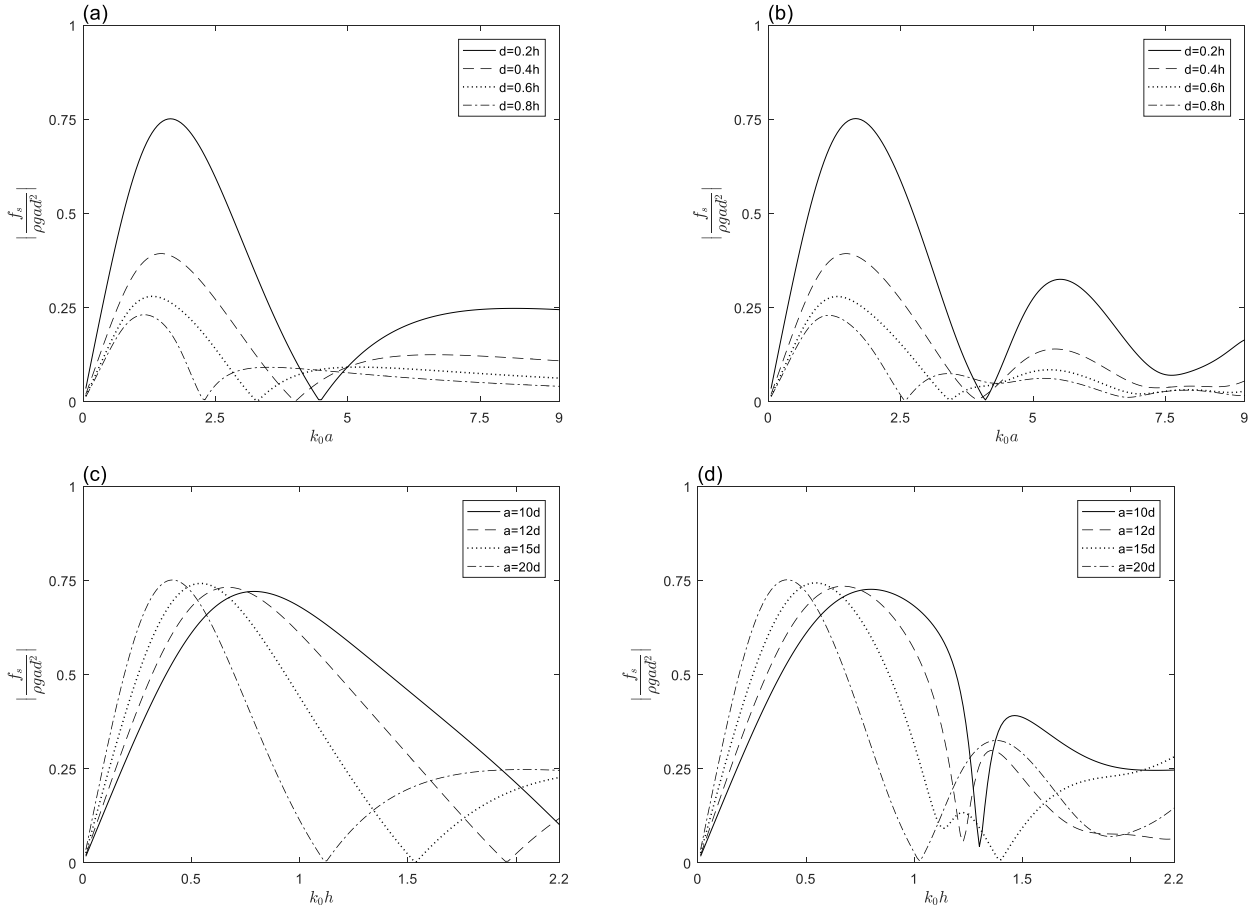


**Figure 8.** Surge force on the ice ridge (a,c) in open water and (b,d) surrounded by level ice ( $\beta_1 = 10^4$ ) . In (a,b)  $h = 0.25a$ ,  $E = 3 \text{ GPa}$ ,  $-\beta_2 = 3.42 \times 10^6$ ,  $---\beta_2 = 2.73 \times 10^7$ ,  $\cdots\beta_2 = 9.23 \times 10^7$ ,  $-\cdot-\beta_2 = 2.18 \times 10^8$ . In (c,d)  $d = 0.2h$ ,  $E = 3 \text{ GPa}$ ,  $\beta_2 = 3.42 \times 10^6$ . Free edge condition is applied to the ice ridge.

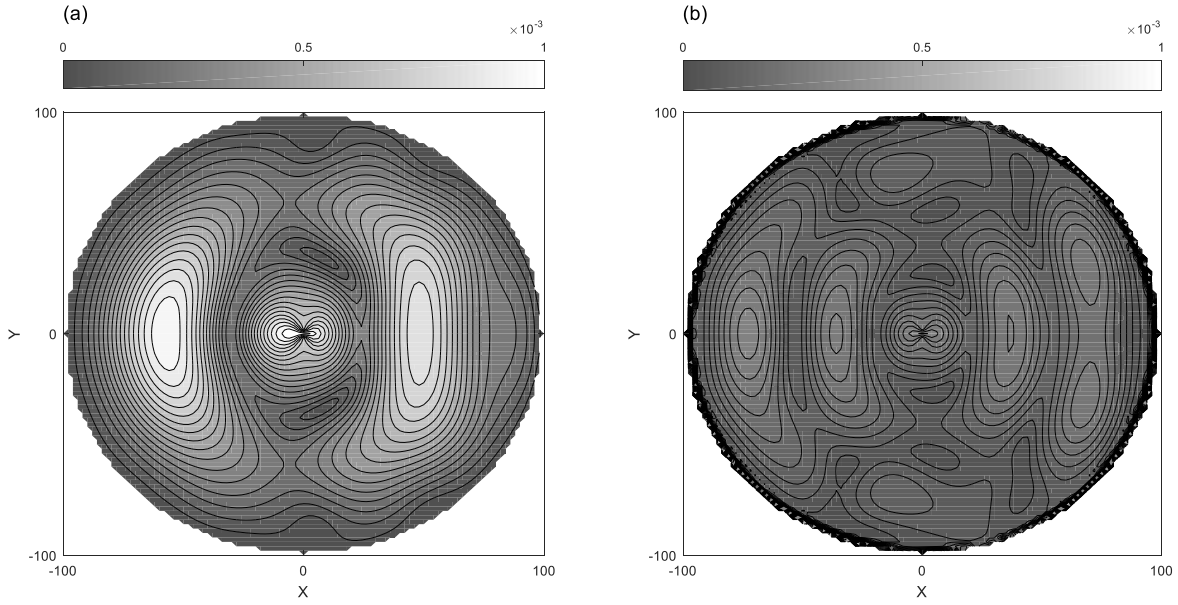


**Figure 9.** Contour plot for bending moment  $M_B$  distribution for (a)  $\beta_1 = 0$  (open water) (a)  $\beta_1 = 10^4$  (embedded in ice cover with free edge boundary condition);  $\beta_2 = 5.34 \times 10^4$  ( $E = 3$  GPa);  $d = 0.05h$ ,  $a = 100$ .

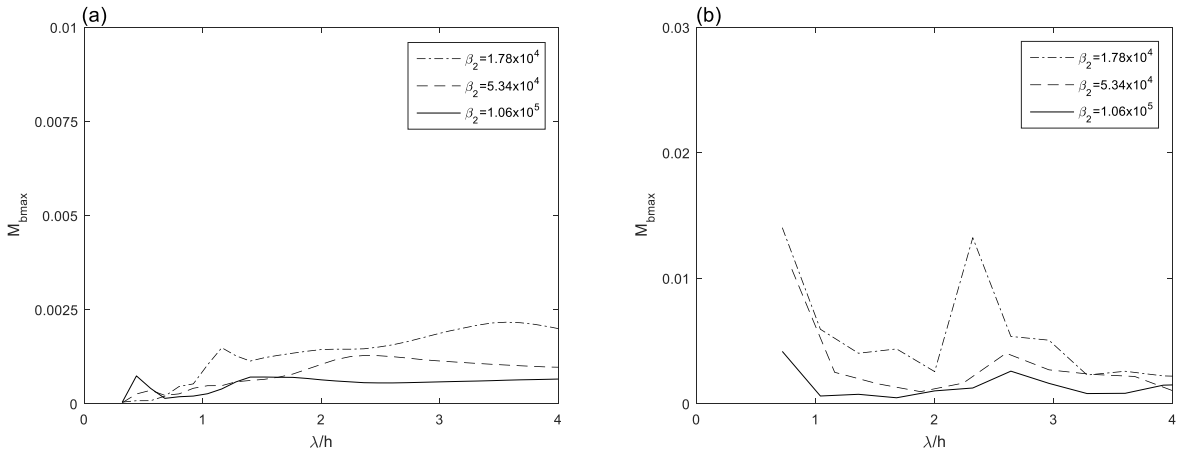


**Figure 10.** Maximum bending moment  $M_{B_{\max}}$  versus nondimensional incoming wavelength  $\lambda/h$  (a)  $\beta_1 = 0$  (open water), (b)  $\beta_1 = 10^4$  (embedded in ice cover with free edge boundary condition);  $d = 0.05h$  and for different  $\beta_2$  ( $E = 1$  GPa, 3 GPa, 6 GPa) with  $h = 25$ ,  $a = 100$ .